



Article

Mechanics Modeling of Residual Stress Considering Effect of Preheating in Laser Powder Bed Fusion

Elham Mirkoohi ^{1,*} , Hong-Chuong Tran ², Yu-Lung Lo ³, You-Cheng Chang ³, Hung-Yu Lin ³ and Steven Y. Liang ¹

¹ Woodruff School of Mechanical Engineering, Georgia Institute of Technology, Atlanta, GA 30332, USA; steven.liang@me.gatech.edu

² Department of Mechanical Engineering, Southern Taiwan University of Science and Technology, Tainan 71005, Taiwan; hongchuong3389@gmail.com

³ Department of Mechanical Engineering, National Cheng Kung University, Tainan City 701, Taiwan; loyl@mail.ncku.edu.tw (Y.-L.L.); n16074425@mail.ncku.edu.tw (Y.-C.C.); n16074409@mail.ncku.edu.tw (H.-Y.L.)

* Correspondence: emirkoohi3@gatech.edu

Abstract: This study aimed at the investigation of the effect of substrate temperature on residual stress in laser powder bed fusion using a physics-based analytical model. In this study, an analytical model is proposed to predict the residual stress through the calculation of preheating affected temperature profile and thermal stress. The effect of preheating is super-positioned with initial temperature in the modeling of temperature profile using a moving heat source approach; the resultant temperature gradient is then employed to predict the thermal stress from a point body load approach. If the thermal stress exceeds the yield strength of the material, then the residual stress under cyclic heating and cooling will be calculated based on the incremental plasticity and kinematic hardening behavior of metal. IN718 is used as a material example to pursue this investigation. To validate the predicted residual stress, experimental measurements are conducted using X-ray diffraction on IN718 samples manufactured via laser powder bed fusion under different process conditions. Results showed that preheating of the substrate could reduce the residual stress in an additively manufactured part due to the reduction in temperature gradient and resultant shrinkage stresses. However, the excessive preheating could have an opposite impact on residual stress accumulation. Moreover, the results confirm that the proposed model is a valuable tool for the prediction of residual stress, eliminating the costly experiments and time-consuming finite element simulations.



Citation: Mirkoohi, E.; Tran, H.-C.; Lo, Y.-L.; Chang, Y.-C.; Lin, H.-Y.; Liang, S.Y. Mechanics Modeling of Residual Stress Considering Effect of Preheating in Laser Powder Bed Fusion. *J. Manuf. Mater. Process.* **2021**, *5*, 46. <https://doi.org/10.3390/jmmp5020046>

Academic Editor: Johan Berglund

Received: 12 March 2021

Accepted: 6 May 2021

Published: 12 May 2021

Publisher's Note: MDPI stays neutral with regard to jurisdictional claims in published maps and institutional affiliations.



Copyright: © 2021 by the authors. Licensee MDPI, Basel, Switzerland. This article is an open access article distributed under the terms and conditions of the Creative Commons Attribution (CC BY) license (<https://creativecommons.org/licenses/by/4.0/>).

Keywords: preheating; PBF-LB; residual stress; IN718; analytical modeling; experimentation

1. Introduction

Metal additive manufacturing (AM), in which the near net shape parts and assemblies are built up from a high precision laser, has become an important technology in the past few years to manufacture 3D components [1]. The metal additive manufacturing can be divided into two main categories of powder feed (PF) system in which the powders are carried out via nozzles; and powder bed fusion (PBF-LB) in which the powders are sat on a bed to be melted selectively [2]. The advantages of AM compared to traditional manufacturing are that the components are built directly without the requirement for specific tooling, enabling the manufacture of complex geometries, which then can reduce the lead time and cost per part. As a result, PBF-LB gaining attention as an assuring technology for the fabrication of large and intricate components for aerospace, marine, and medical companies [3,4].

The residual stress resulting from rapid heating and cooling cycles in PBF-LB is not well understood yet. Each process parameter can considerably change the residual stress distribution. This is a very important issue in additive manufacturing of metallic components since it not only degrades the dimensional accuracy and mechanical performance

of the component, but also increases the manufacturing cost due to necessity for post-processing treatments [5]. It is therefore important to understand and control the residual stress by the optimization of process parameters.

Residual stress induced by laser powder bed fusion (PBF-LB) can surpass the yield strength of the metal [6]. Such high residual stress buildup could affect the microstructure and mechanical properties of the fabricated part [7]. There are thermal and mechanical treatments available to reduce residual stress. They include in situ preheating of the substrate in which the part is built on top of it, post-processing heat treatment, peening, and pre-setting [8]. Preheating involves raising the temperature of the substrate, in which the part is built on top of it above the ambient temperature. Preheating could improve the additive-manufacturability of the parts since it degrades the temperature gradient, cooling rates, and reduces the magnitude of thermal stresses. On the other hand, an excessive amount of preheating could have an opposite impact on final performance of the manufactured part. The excessive amount of preheating could result in segregation of embrittling impurity elements to the grain boundaries. It also causes significant grain coarsening in the melt pool area and heat-affected zone (HAZ) and results in the creation of a wider zone of grain boundary liquification. These partly melted zones have very poor ductility and are quite sensitive to cracking as explained by Lin et al. [9]. Therefore, magnitude of the preheating temperature plays an important role on the final performance of the additively manufactured part.

Analytical models play a significant role in the study of thermo-mechanical behavior in metal AM. The rationale for performing analytical modeling of additive manufacturing processes is to reduce the experimentation needed to optimize the process parameters [10]. In addition, it offers high-performance computing. For instance, the simulation of residual stress considering multi-layer and multi-scan aspects of AM process using the proposed model takes less than two and a half minutes to be completed using a 2.3 GHz core i5 laptop compared to hours of calculations using finite element modeling since it involves no iteration, nor meshing. Moreover, such models can then be extended to model the microstructure of the additively manufactured part. For example, Tabei et al. [11] used the thermo-mechanical analytical model to predict the microstructure of an additively manufactured part, and Ji et al. [12] used a similar model to predict the grain size of an additively manufactured part.

Finite element analysis (FEA) has been an active area of research for modeling of AM process. Nick et al. [13] used FEA to model the effect of a deposition pattern on residual stress on laser-deposited 1117 steel. In this modeling, they did not consider the effect of latent heat; the entire layer is heated up and then cooled down after deposition instead of using a moving heat source, and the effect of the layer addition and multi-scan aspect of AM is also not considered. Alimardani et al. [14] proposed a numerical model to investigate the effect of pre-heating on residual stress in additive manufacturing of 304 L stainless-steel. They concluded that the pre-heating could reduce the thermal stress and subsequent residual stress. In this modeling, the results are not validated. Chew et al. [15] developed a FE model to predict the residual stress in a single and multiple bead laser deposition. They have validated their results by conducting experimental residual stress using X-ray diffraction. The results showed quantitative agreement with experimental measurements, however, the measurement results are obtained only at the center of clad. Ding et al. [16] verified the bulk residual stress distribution simulated by a finite element model using neutron diffraction for samples up to three layers. While the predicted and measured residual stresses are in good agreement for the second and third layers, the simulation dramatically underestimated the residual stress for the first layer. Ali et al. experimentally investigated the effect of preheating on yield strength and ductility of the Ti6Al4V. They found that increasing the temperature of the bed to 570 °C could improve the yield strength and elongation of the component by 3.2% and 66.6%, respectively [17]. Buchbinder et al. investigated the effect of preheating on distortion of the additively manufactured components. They concluded that the preheating of substrate to 250 °C resulted

in elimination of distortion from 10.6 mm (without preheating) [18]. Sames et al. indicated that the highest stress concentration is located near the interface between substrate and SLM-processed part. These results indicate that the interface between substrate and part is the locations where the part has more possibility to delaminate during SLM process [19].

To the best of the authors' knowledge, there is no work that specifically models the effect of preheating of substrate on residual stress in metal AM and validates that via experimentation.

The purpose of the current work is to investigate the impact of preheating temperature on residual stress formation during additive manufacturing of Inconel 718 (IN718). A fully coupled thermo-mechanical model simulates the residual stress distribution using incremental plasticity and kinematic hardening behavior of the metal through the prediction of a temperature field by considering the effect of preheating in the modeling by superposing the preheating temperature with initial temperature.

2. Methodology

The first step in mechanics modeling of AM process is to predict the temperature field induced by a laser as shown in Figure 1. In this modeling approach, a transient moving point heat source approach is used to simulate the laser. The heat loss due to convection, radiation, and conduction is also considered in this modeling [20]. To consider the effect of preheating, the constant preheating temperature is added to the moving profile as the following:

$$T_{final} = T - T_{loss} = \frac{P\eta}{4\pi KR(T-T_0)} \times \left\{ \exp\left(\frac{-V(R+x)}{2D}\right) - ls \left[h(T - T_0) + \epsilon\sigma(T^4 - T_0^4) + \frac{K(T-T_0)}{R} \right] \right\} + T_{preheating} \tag{1}$$

where P is the laser power, η represents the absorption coefficient, V is scan speed, D is thermal diffusivity, and T_0 is the initial temperature. More explanation and validation of the proposed temperature model can be found in the previous work of these authors in [9,20]. It should be noted that both modeling and experiments follow each other in terms of material used for substrate and build part.

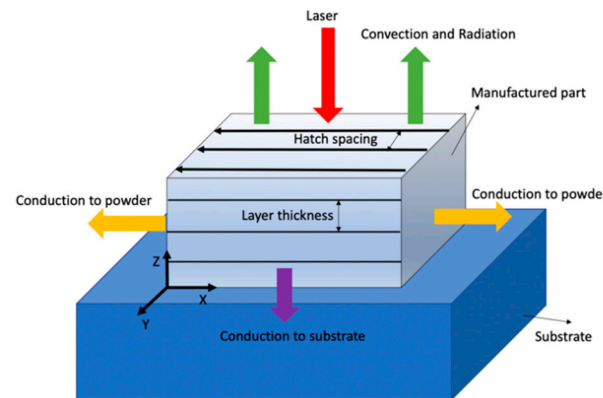


Figure 1. Heat transfer mechanisms in laser powder bed fusion.

Calculated temperature gradient from thermal modeling is used as an input to predict the thermal stress in the AM parts as explained in previous work of authors [21] using Green's function of stresses due to the point body load.

In this process, high strain, strain rate, and temperature will be generated. The Johnson–Cook materials' consecutive model is used to capture these effects as follows:

$$\sigma = \left(A + B\epsilon_{eff}^p \right)^n \left(1 + C \ln\left(\frac{\dot{\epsilon}_{eff}^p}{\dot{\epsilon}_0}\right) \right) \left(1 - \left[\frac{T - T_{preheating}}{T_m - T_{preheating}} \right]^m \right) \tag{2}$$

where ϵ_{eff}^p is the effective plastic strain, $\dot{\epsilon}_{eff}^p$ is the effective plastic strain rate, T is the temperature of material, T_m is the melting point of material, and $T_{preheating}$ is the substrate's temperature. The terms A , B , C , n , m , and $\dot{\epsilon}_0$ are the material constants, which are listed in Table 1 for IN718 material.

Table 1. Modified Johnson–Cook parameters for IN718 [22].

A (MPa)	B (MPa)	C	n	m	$\dot{\epsilon}_0$
980	1370	0.02	0.164	1.03	1

The yielding criterion is obtained for an isotropic material. Kinematic hardening is considered by employing the backstress tensor (α_{ij})

$$F_{yeild} = \frac{3}{2}(S_{ij} - \alpha_{ij})(S_{ij} - \alpha_{ij}) - k^2 = 0 \tag{3}$$

where $S_{ij} = \sigma_{ij} - (\sigma_{kk}/3)\delta_{ij}$ is the deviatoric stress.

If $F_{yeild} > 0$, incremental plastic strains are calculated and accumulated during the stress history to determine the total plastic strains using modified McDowell algorithm [23].

$$\psi \begin{cases} \frac{1}{E} [\dot{\sigma}_{xx} - \nu(\dot{\sigma}_{yy} - \dot{\sigma}_{zz})] + \alpha\Delta T + \frac{1}{h} (\dot{\sigma}_{xx}n_{xx} + \dot{\sigma}_{yy}n_{yy} + \dot{\sigma}_{zz}n_{zz} + 2\dot{\sigma}_{xz}^*n_{xz})n_{xx} = \\ \frac{1}{E} [\dot{\sigma}_{xx}^* - \nu(\dot{\sigma}_{yy} - \dot{\sigma}_{zz}^*)] + \alpha\Delta T + \frac{1}{h} (\dot{\sigma}_{xx}^*n_{xx} + \dot{\sigma}_{yy}n_{yy} + \dot{\sigma}_{zz}^*n_{zz} + 2\dot{\sigma}_{xz}^*n_{xz})n_{xx} \\ \frac{1}{E} [\dot{\sigma}_{yy} - \nu(\dot{\sigma}_{xx} - \dot{\sigma}_{zz})] + \alpha\Delta T + \frac{1}{h} (\dot{\sigma}_{xx}n_{xx} + \dot{\sigma}_{yy}n_{yy} + \dot{\sigma}_{zz}n_{zz} + 2\dot{\sigma}_{xz}^*n_{xz})n_{yy} = 0 \\ \dot{\sigma}_{yy} = \frac{1}{2}(\dot{\sigma}_{xx} + \dot{\sigma}_{zz}) \end{cases} \tag{4}$$

where, $\dot{\sigma}_{xx}^*$, $\dot{\sigma}_{zz}^*$, $\dot{\sigma}_{xz}^*$ are the elastic thermal stresses calculated from [24]. In McDowell model [6], a hybrid function (ψ) is proposed, which depends on the instantaneous value of the modulus ratio $\frac{h}{G}$ as:

$$\psi = 1 - \exp\left(-\zeta \frac{3h}{2G}\right) \tag{5}$$

where $\zeta = 0.15$ is the algorithm constant, h is the plastic modulus, and $G = \frac{E}{2(1+\nu)}$ is the elastic shear modulus. Three systems of equations are solved simultaneously for $\dot{\sigma}_{xx}$, $\dot{\sigma}_{yy}$, and $\dot{\sigma}_{zz}$ for each elastic-plastic increment of strain.

3. Experimental Procedure

The Nd: YAG laser with the laser spot size of $D4sigma = 54 \mu\text{m}$ and laser power of 50 W to 400 W was set up on a commercial Tong Tai AM250 SLM machine to manufacture high-density components using variable pre-heating temperatures. The IN718 powders with the powder size distribution of $d10 = 17.51 \mu\text{m}$; $d50 = 31.44 \mu\text{m}$; $d90 = 52.21 \mu\text{m}$ was used. The range of scan speed varied between 100 mm/s to 2000 mm/s. The processing conditions used to fabricate samples are listed in Table 2. To make sure that the selected process parameters would result in a high-density sample, the density of the fabricated samples was measured and listed in Table 3. For measuring the density, each sample was sawed in half. Then, the obtained cross-sections were polished, and their images were taken by a digital camera attached to the microscope. For each sample, the images were captured at five different locations of the cross-section, and the ImageJ software was employed to calculate the relative density by evaluating the ratio between total pore areas and the total cross-sectional area. The calculated relative density from the five images was used to determine the mean value of the relative density of the fabricated samples. Figure 2a,b show the cross-section images corresponding to the parameters for samples 1 and 2 specified in Table 2, respectively. The statistical results of relative density corresponding to each set of polished samples are shown in Table 3. It should be noted that the IN718 substrate has the dimension of $20 \times 10 \times 10 \text{ mm}$.

Table 2. Process Parameters Designed for the fabrication of IN718 specimens using PBF-LB.

No.	Laser Power (W)	Scanning Speed (mm/s)	Powder Layer Thickness (μm)	Hatch Spacing (μm)	Number of Scans	Pre-Heating (°C)	Rotation Angle of Scan Vector between Layers (°)
1	150	600	30	100	50	No	67
2	150	600	30	100	50	100	67

Table 3. Measured density of fabricated samples.

No.	Average Density	Standard Deviations
1	99.96%	0.017%
2	99.94%	0.02%

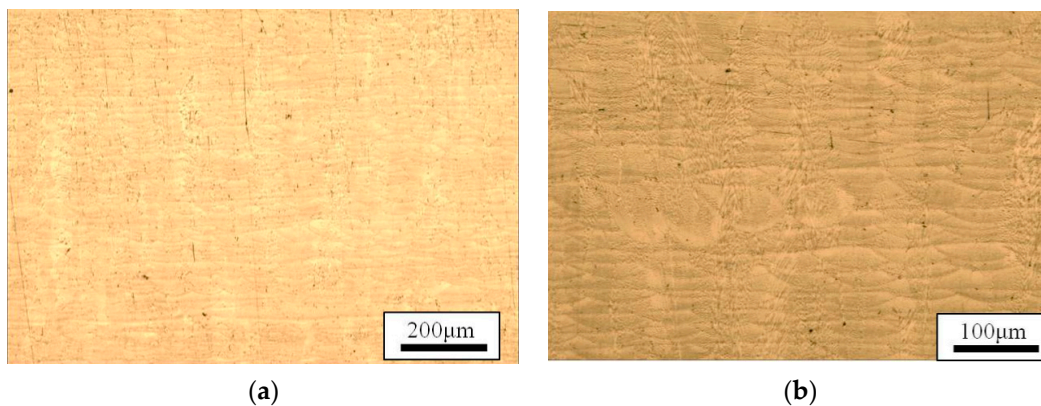


Figure 2. Polished cross-sections corresponding to two different processing conditions (a) Sample No. 1; (b) Sample No. 2.

In these fabricated samples, the laser power, scan speed, layer thickness, and scan pattern are kept the same, and pre-heating condition is changed to investigate the impact of pre-heating on residual stress. For each set of parameters specified in Table 2, there were three samples fabricated. The as-built samples were then removed from the base plate using the electrical discharge machining (EDM).

The residual stress on the side walls of the samples, as illustrated in Figure 3, was measured by a commercial X-Ray Diffractions machine (D8 Discover Bruker) using the $\sin^2\Psi$ method [25,26]. The coordinates and location of measured points are shown in Table 4. For each point shown in Figure 3, residual stresses along the build direction (z direction), and along the scan direction (x direction) were measured. The parameters for XRD measurement are specified in Table 5. It is noted that for each set of parameters and each point shown in Figure 3, the XRD measurements were performed on three fabricated samples and the results were averaged.

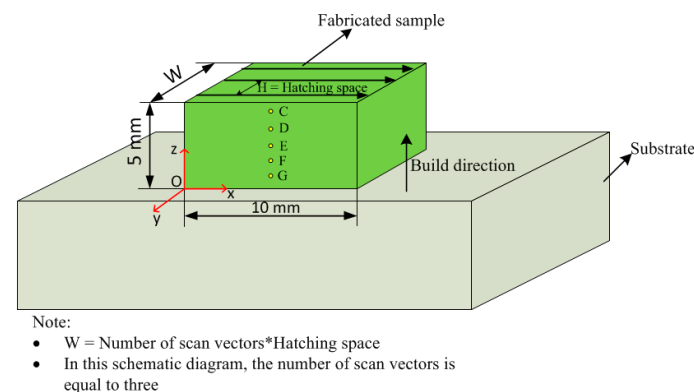


Figure 3. Schematic diagram illustrating the definition of processing parameters.

Table 4. Coordinates of the measured points using XRD.

C	x = 5 mm; y = 0; z = 4.5 mm
D	x = 5 mm; y = 0; z = 3.5 mm
E	x = 5 mm; y = 0; z = 2.5 mm
F	x = 5 mm; y = 0; z = 1.5 mm
G	x = 5 mm; y = 0; z = 0.5 mm

Table 5. Parameters for XRD measurements.

Focus	1.0 mm
Radiation	Cu K α
Lattice plane (hkl) [26]	{411}
2θ	145 $^\circ$
Ψ-tilting	0 $^\circ$ to 45 $^\circ$ in 6 steps each
Young modulus [27]	199,955 MPa
Poisson ration [27]	0.29

4. Results and Discussion

The proposed thermo-mechanical model calculates the residual stress from incremental plasticity approach in the metal additive manufacturing process through the prediction of temperature profile and thermal stress as explained in the methodology section. A moving point heat source approach is employed to predict the temperature field by considering the effect of temperature dependent material properties of IN718 samples as listed in Table 6. In addition, the effects of multi-layer and multi-scan aspects of PBF-LB process, the heat loss due to convection, conduction, and radiation from boundaries, as well as energy needed for solid state phase change, are considered in the modeling of temperature field.

Table 6. Temperature-dependent material properties of IN718 (Temperature is in $^\circ\text{C}$).

Density g/cm3 $\rho = 8.19 - 39.2 \times 10^{-2}T$ $\rho = 7.40 - 88.0 \times 10^{-2}(T - 1200)$	25 < T \leq 1170 T > 1170
Thermal $k = 39.73 - 24.0 \times 10^{-3} T + 2 \times 10^{-3} T^{-2}$ $k = 29.6$	25 < T < 1170 T > 1170
Specific $C_p = 420.24 + 0.026T - 4 \times 10^{-6} T^2$ $C_p = 650$	25 < T \leq 1170 T > 1170
Thermal expansion 1/$^\circ$ $\alpha = -9 \times 10^{-13} T^2 - 7.7 \times 10^{-9}T + 1.1 \times 10^{-5}$ $\alpha = 1.8 \times 10^{-5}$	25 < T \leq 1100 T > 1100
Elastic modulus GPa $E = 5.2 \times 10^{-5} T^2 - 0.088T + 1.6 \times 10^2$ $E = 3.1 \times 10^{-5} T^2 - 0.23T + 2.9 \times 10^2$	25 < T \leq 798 798 < T < 2500
Yield strength MPa $\sigma_Y = -9 \times 10^{-10} T^4 - 1.2 \times 10^{-6} T^3 + 0.00026 T^2 - 0.23T + 3.2 \times 10^2$	25 < T < 2500
Poisson's ratio $\nu = -4.8 \times 10^{-10} T^3 - 8.8 \times 10^{-7} T^2 - 0.00031T + 0.31$	25 < T < 2500

Figure 4a,b demonstrate the predicted temperature profile for the sample with no preheating, and with a pre-heating temperature of 100 $^\circ\text{C}$, respectively. The comparison of

these plots shows that the overall temperature is higher for sample 2 which is preheated to 100 °C, however, the temperature gradient is lower due to the preheating’s effect. Thus, looking at these figures, the residual stress is expected to be lower when the substrate is preheated to some level.

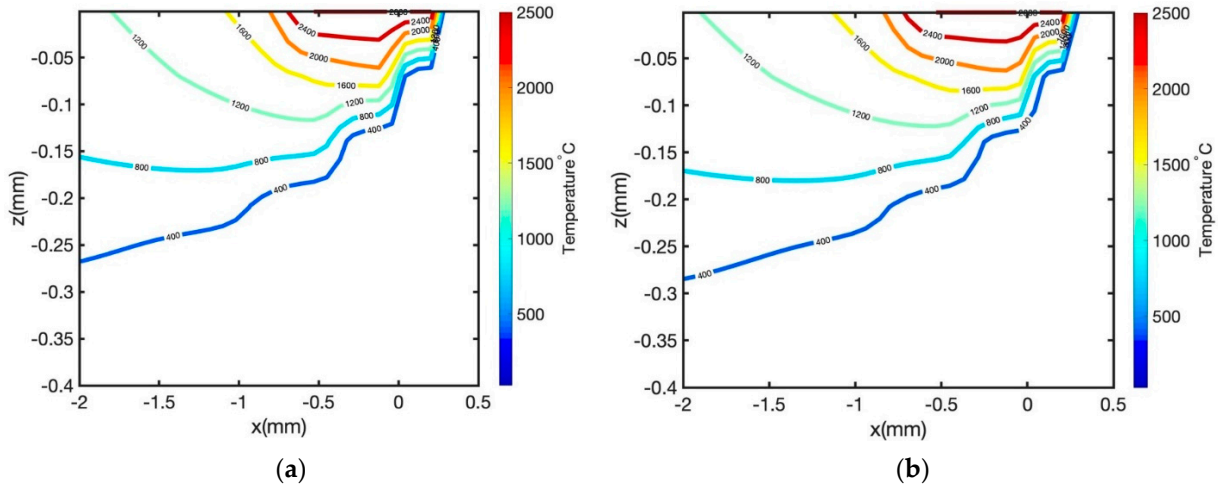


Figure 4. Predicted temperature profile for IN718 sample fabricated via PBF-LB with (a) no pre-heating of the substrate (Sample 1 in Table 2) and (b) pre-heating of the substrate to 100 ° (Sample 2 in Table 2).

Figures 5 and 6 illustrate the predicted and measured residual stress along the scan direction (σ_x), and along the build direction (σ_z), respectively.

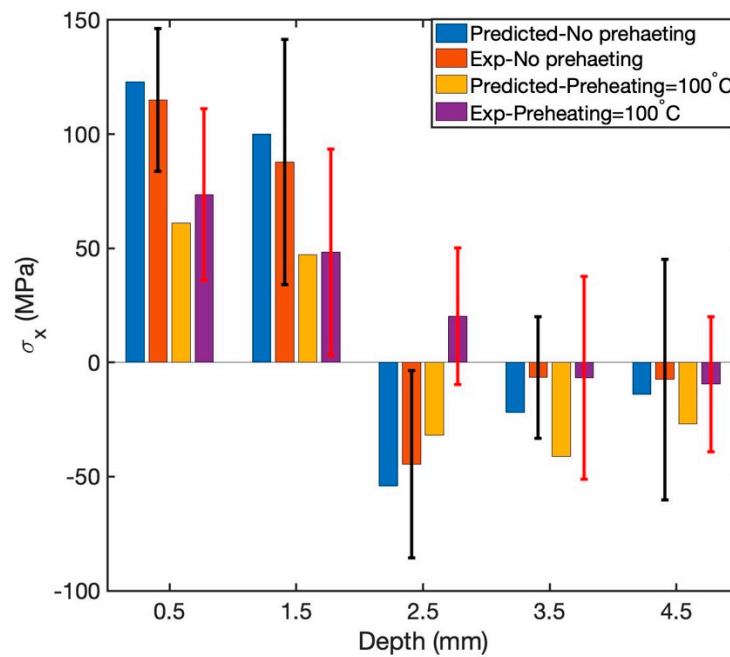


Figure 5. Comparison of the predicted and measured residual stress along the scan direction.

As shown in Figure 5, residual stresses at five different depths are calculated and compared to experimental measurements for two cases where for sample 1, the substrate is not preheated, and it is at ambient temperature, and for the sample 2, the substrate is preheated to 100 °C. The black error bar shows the experimental residual stress measurements for no-pre-heating of the substrate, and the red one shows the experimental measurements of residual stress for the case where the substrate is preheated to 100 °C. The predicted residual stress shows that the tensile residual stress along the scan direction has dropped

by half. Therefore, the preheating of the substrate has a substantial effect on residual stress build-up. The comparison of the predicted and measured residual stress for both samples are in good quantitative and qualitative agreements with the maximum error of 12%.

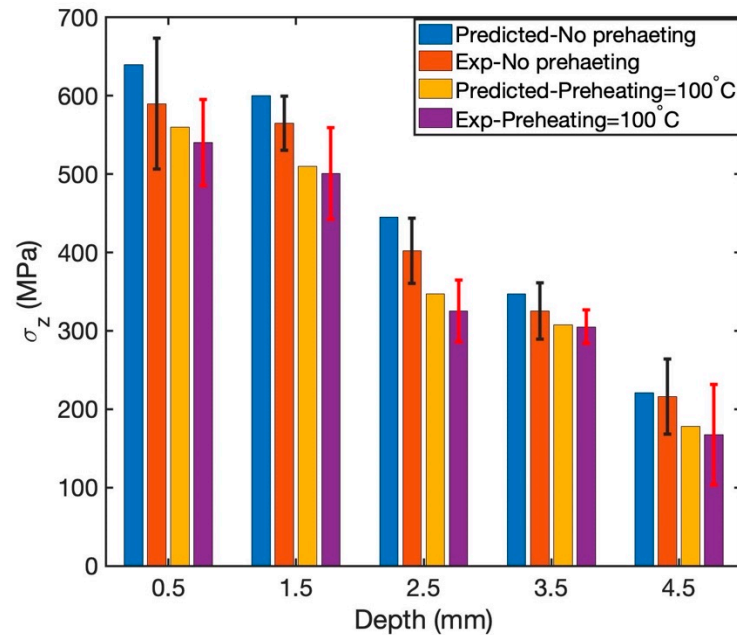


Figure 6. Comparison of the predicted and measured residual stress along the build direction.

Figure 6 demonstrates the predicted and measured residual stress in the build direction. As shown in this figure, the average residual stress in the build direction has reduced by around 14% in both modeling and experiments when the substrate is preheated to 100 °C.

The comparison of the results along the scan direction and build direction shows that the magnitude of residual stress along the build direction is higher than that along the scan direction. This observation is consistent with the experimental findings and simulation results reported in [5]. In addition, it is observed that pre-heating has more influence on residual stress along the scan direction compared to that along the build direction. This could be due to the fact that the microstructural evolution along the build direction and scan direction shows different behavior, thus affecting the material properties and residual stress formation.

5. Sensitivity Analysis

Since the proposed model was validated, a sensitivity analysis was performed to investigate the effect of preheating in a broader range. In this sensitivity analysis, the laser power was 150 W, the scan speed was 600 mm/s, the layer thickness was 30 μm, the hatching space was 100 μm, the number of scans was 50, and the preheating temperature ranges were from 50 °C to 500 °C. As can be seen in Figures 7 and 8, the results show two different stages. One from 50 °C to 200 °C in which a rapid drop in residual stress is observed, and the second stage from 200 °C to 500 °C in which the residual stress has increased. With the current substrate's material (IN718) and dimension, our hypothesis was that the increase in temperature above 200 °C would result in accumulation of heat, thus adversely impacting the residual stress. This result also demonstrates the importance of the substrate's dimension and material. More investigation is required to understand the impact of these parameters on residual stress.

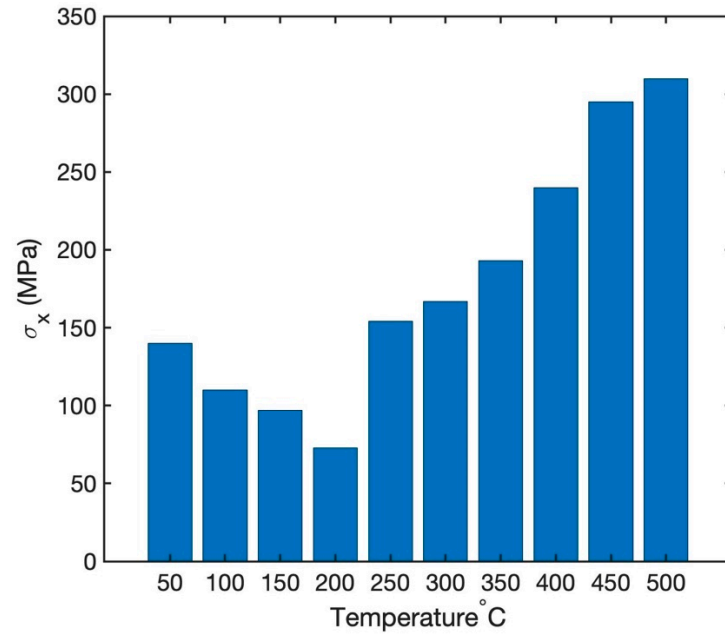


Figure 7. Effect of pre-heating on residual stress build up in PBF-LB of IN718 along the scan direction.

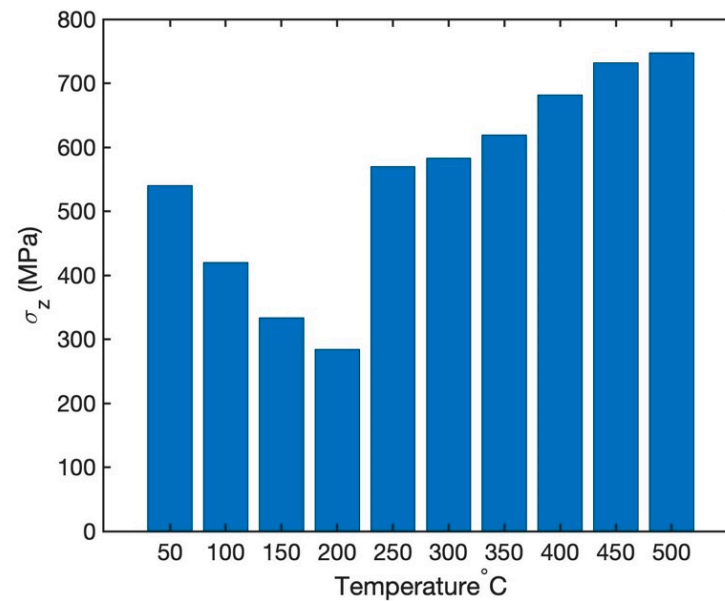


Figure 8. Effect of pre-heating on residual stress build up in PBF-LB of IN718 along the build direction.

Thus, the results show the importance of the optimization of the preheating temperature in achieving a desired residual stress and final performance of the manufactured part.

6. Conclusions

A physics-based analytical model is proposed to investigate the effect of preheating on residual stress build-up in PBF-LB. The residual stress is predicted by calculating the temperature field using a moving point heat source approach by considering the effects of heat loss, temperature-dependent material properties, multi-layer and multi-scan aspects of the process, energy needed for solid-state phase change, and preheating temperature. The high-temperature gradient in this process induces high thermal stress which is calculated using Green’s function of stresses due to the point body load. The thermal stress usually exceeds the yield strength of the material, thus, a consecutive model, known as the Johnson–Cook model is employed to capture the yield threshold. Then, as

a result of cyclic rapid heating and cooling and the fact that the material is yielded and experiences the plasticity, the residual stress is calculated from incremental plasticity and kinematic hardening behavior of the metal.

The residual stresses are predicted for two cases where the substrate is at ambient temperature, and for another case where the substrate is preheated to 100°C. The results showed that residual stress decreased when the substrate was preheated. Moreover, the drop in residual stress along the scan direction was higher than that along the build direction. This is due to the fact that the heat transfer mechanisms and the subsequent microstructural evolution are quite different in these two directions, resulting in variation of behaviors. The results are validated by fabricating samples under different preheating conditions using an PBF-LB machine. X-ray diffraction was then used to measure the residual stress of the samples. Good quantitative and qualitative agreement is observed between predicted and measured residual stress. It should be noted that the obtained results have been confirmed experimentally for IN718 substrate with specific dimensions. The change in material and dimension would have an impact on residual stress formation due to the change in heat conduction.

In addition, a sensitivity analysis is performed to investigate the effect of preheating in a broader range. The results showed that the preheating temperature could reduce the residual stress, however, an excessive amount of preheating has an opposite impact on residual stress formation since this could result in reduction of yield strength due to the grain coarsening of the melt zone and heat-affected zone, thus increasing the residual stress build-up.

Author Contributions: Conceptualization, E.M.; methodology, E.M.; software, E.M.; validation, E.M., H.-C.T., Y.-L.L., H.-Y.L., Y.-C.C.; formal analysis, E.M., H.-C.T., Y.-L.L., H.-Y.L., Y.-C.C.; investigation, E.M., H.-C.T., Y.-L.L., H.-Y.L., Y.-C.C.; data curation, E.M., H.-C.T., Y.-L.L., H.-Y.L., Y.-C.C.; writing—original draft preparation, E.M.; writing—review and editing, E.M.; visualization, E.M.; supervision, S.Y.L. All authors have read and agreed to the published version of the manuscript.

Funding: This research received no external funding.

Data Availability Statement: Data sharing not applicable.

Acknowledgments: The experimental data were financially supported by the “Intelligent Manufacturing Research Center” (iMRC) from The Featured Areas Research Center Program within the framework of the Higher Education Sprout Project by the Ministry of Education (MOE) in Taiwan.

Conflicts of Interest: The authors declare no conflict of interest.

References

1. Bartlett, J.L.; Li, X. An overview of residual stresses in metal powder bed fusion. *Addit. Manuf.* **2019**, *27*, 131–149. [[CrossRef](#)]
2. Bagg, S.D.; Sochalski-Kolbus, L.M.; Bunn, J.R. The effect of laser scan strategy on distortion and residual stresses of arches made with selective laser melting. In Proceedings of the American Society of Precision Engineering (ASPE) 2016 Summer Topical Meeting: Dimensional Accuracy and Surface Finish in Additive Manufacturing, Raleigh, NC, USA, 27–30 June 2016.
3. Gu, D. *Laser Additive Manufacturing of High-Performance Materials*; Springer: Berlin/Heidelberg, Germany, 2015.
4. Gorji, N.E.; O’Connor, R.; Brabazon, D. X-ray Tomography, AFM and Nanoindentation Measurements for Recyclability Analysis of 316L Powders in 3D Printing Process. *Procedia Manuf.* **2020**, *47*, 1113–1116. [[CrossRef](#)]
5. Ganeriwala, R.K.; Strantz, M.; King, W.E.; Clausen, B.; Phan, T.Q.; Levine, L.E.; Brown, D.W.; Hodge, N.E. Evaluation of a thermomechanical model for prediction of residual stress during laser powder bed fusion of Ti-6Al-4V. *Addit. Manuf.* **2019**, *27*, 489–502. [[CrossRef](#)]
6. Mirkoohi, E.; Dobbs, J.R.; Liang, S.Y. Analytical modeling of residual stress in direct metal deposition considering scan strategy. *Int. J. Adv. Manuf. Technol.* **2020**, *106*, 4105–4121. [[CrossRef](#)]
7. Sharma, R.; Kumar, A. Track-Scale Simulations of Selective Laser Melting to Investigate Development and Mitigation of Thermal Stresses. *Lasers Manuf. Mater. Process.* **2019**, *6*, 464–492. [[CrossRef](#)]
8. Cao, J.; Gharghour, M.A.; Nash, P. Finite-element analysis and experimental validation of thermal residual stress and distortion in electron beam additive manufactured Ti-6Al-4V build plates. *J. Mater. Process. Technol.* **2016**, *237*, 409–419. [[CrossRef](#)]
9. Lin, Y.-C.; Lee, K. Effect of preheating on the residual stress in type 304 stainless steel weldment. *J. Mater. Process. Technol.* **1997**, *63*, 797–801. [[CrossRef](#)]

10. Mirkoohi, E.; Sievers, D.E.; Garmestani, H.; Chiang, K.; Liang, S.Y. Three-dimensional semi-elliptical modeling of melt pool geometry considering hatch spacing and time spacing in metal additive manufacturing. *J. Manuf. Process.* **2019**, *45*, 532–543. [[CrossRef](#)]
11. Tabei, A.; Mirkoohi, E.; Garmestani, H.; Liang, S. Modeling of texture development in additive manufacturing of Ni-based superalloys. *Int. J. Adv. Manuf. Technol.* **2019**, *103*, 1057–1066. [[CrossRef](#)]
12. Ji, X.; Mirkoohi, E.; Ning, J.; Liang, S.Y. Analytical modeling of post-printing grain size in metal additive manufacturing. *Opt. Lasers Eng.* **2020**, *124*, 105805. [[CrossRef](#)]
13. Nickel, A.; Barnett, D.; Prinz, F. Thermal stresses and deposition patterns in layered manufacturing. *Mater. Sci. Eng. A* **2001**, *317*, 59–64. [[CrossRef](#)]
14. Alimardani, M.; Toyserkani, E.; Huissoon, J.P. A 3D dynamic numerical approach for temperature and thermal stress distributions in multilayer laser solid freeform fabrication process. *Opt. Lasers Eng.* **2007**, *45*, 1115–1130. [[CrossRef](#)]
15. Chew, Y.; Pang, J.H.; Bi, G.; Song, B. Thermo-mechanical model for simulating laser cladding induced residual stresses with single and multiple clad beads. *J. Mater. Process. Technol.* **2015**, *224*, 89–101. [[CrossRef](#)]
16. Ding, J.; Colegrove, P.; Mehnen, J.; Ganguly, S.; Almeida, P.S.; Wang, F.; Williams, S. Thermo-mechanical analysis of Wire and Arc Additive Layer Manufacturing process on large multi-layer parts. *Comput. Mater. Sci.* **2011**, *50*, 3315–3322. [[CrossRef](#)]
17. Ali, H.; Ma, L.; Ghadbeigi, H.; Mumtaz, K. In-situ residual stress reduction, martensitic decomposition and mechanical properties enhancement through high temperature powder bed pre-heating of Selective Laser Melted Ti6Al4V. *Mater. Sci. Eng. A* **2017**, *695*, 211–220. [[CrossRef](#)]
18. Buchbinder, D.; Meiners, W.; Pirch, N.; Wissenbach, K.; Schrage, J. Investigation on reducing distortion by preheating during manufacture of aluminum components using selective laser melting. *J. Laser Appl.* **2014**, *26*, 012004. [[CrossRef](#)]
19. Sames, W.J.; List, F.A.; Pannala, S.; Dehoff, R.R.; Babu, S.S. The metallurgy and processing science of metal additive manufacturing. *Int. Mater. Rev.* **2016**, *61*, 315–360. [[CrossRef](#)]
20. Ning, J.; Mirkoohi, E.; Dong, Y.; Sievers, D.E.; Garmestani, H.; Liang, S.Y. Analytical modeling of 3D temperature distribution in selective laser melting of Ti-6Al-4V considering part boundary conditions. *J. Manuf. Process.* **2019**, *44*, 319–326. [[CrossRef](#)]
21. Mirkoohi, E.; Sievers, D.E.; Garmestani, H.; Liang, S.Y. Thermo-mechanical modeling of thermal stress in metal additive manufacturing considering elastoplastic hardening. *CIRP J. Manuf. Sci. Technol.* **2020**, *28*, 52–67. [[CrossRef](#)]
22. Kobayashi, T.; Simons, J.W.; Brown, C.S.; Shockey, D.A. Plastic flow behavior of Inconel 718 under dynamic shear loads. *Int. J. Impact Eng.* **2008**, *35*, 389–396. [[CrossRef](#)]
23. McDowell, D. An approximate algorithm for elastic-plastic two-dimensional rolling/sliding contact. *Wear* **1997**, *211*, 237–246. [[CrossRef](#)]
24. Mirkoohi, E.; Dobbs, J.R.; Liang, S.Y. Analytical mechanics modeling of in-process thermal stress distribution in metal additive manufacturing. *J. Manuf. Process.* **2020**, *58*, 41–54. [[CrossRef](#)]
25. Nadammal, N.; Kromm, A.; Saliwan-Neumann, R.; Farahbod, L.; Haberland, C.; Portella, P.D. Influence of support configurations on the characteristics of selective laser-melted inconel 718. *JOM* **2018**, *70*, 343–348. [[CrossRef](#)]
26. Prevey, P.S. X-ray diffraction residual stress techniques. *ASM Int. ASM Handb.* **1986**, *10*, 380–392.
27. Yang, Y.P.; Jamshidinia, M.; Boulware, P.; Kelly, S.M. Prediction of microstructure, residual stress, and deformation in laser powder bed fusion process. *Comput. Mech.* **2018**, *61*, 599–615. [[CrossRef](#)]